






Article

# Experimental study of the summation of flicker caused by wind turbines.

Koldo Redondo , José Julio Gutiérrez , Izaskun Azcarate , Purificación Saiz , Luis Alberto Leturiondo and Sofía Ruiz de Gauna 

University of the Basque Country (UPV/EHU)

Department of Communications Engineering

Current address: Plaza Ingeniero Torres Quevedo 1 48013 - Bilbao - Spain

\* Correspondence: koldo.redondo@ehu.es; Tel.: +34 94 601 3901

Version May 21, 2019 submitted to Preprints

**Abstract:** Integration of wind energy into the grid faces a great challenge regarding power quality. The International Electrotechnical Commission (IEC) 61400-21 standard defines the electrical characteristics that need to be assessed in a Wind Turbine (WT), as well as the procedure to measure the disturbances produced by the WT. One of the parameters to be assessed are voltage fluctuations or flicker. To estimate the flicker emission of a Wind Power Plant (WPP), the standard establishes that a quadratic exponent should be used in the summation of the flicker emission of each WT. This exponent was selected based on studies carried out in WPPs with type I and II WTs. Advances in wind turbines technology have reduced their flicker emission, mainly thanks to the implementation of power electronics for the partial or total management of the power injected into the grid. This work is based on measurements from a WPP with 16 type III WTs. The flicker emission of a single WT and of the WPP were calculated. Low flicker emission values at the Point of Common Coupling (PCC) of the WPP were obtained. The flicker estimation at the PCC, based on the measurement from a single WT, was analyzed using different exponents. The results show that a cubic summation performs better than the quadratic one in the estimation of the flicker emission of a WPP with type III WTs.

**Keywords:** Power Quality; Wind Power Plant; Voltage Fluctuations

## 1. Introduction

Wind energy represents an increasing proportion of the globally produced energy [1,2]. Power quality control is required to not compromise the quality of the supply network with the integration into the grid of this renewable source [3]. The International Electrotechnical Commission (IEC) 61400-21 standard defines the procedures for measuring and assessing the power quality in grid connected Wind Turbines (WTs) [4]. The revision of the standard in force is being addressed within the Maintenance Team TC88/MT21 of IEC, whose work will lead to the release of a new edition of the standard separated in two parts: Part 1 for testing WTs, and Part 2 for testing Wind Power Plants (WPPs).

The quantities that shall be stated for characterizing the power quality of a single WT according to the standard are: voltage fluctuations, current harmonics, interharmonics, high frequency components, voltage drop response, power control (active and reactive power), grid protection and reconnection time. The literature gathers several works about the measurement, modelling and control of these disturbances and how to minimize their impact [5–7].

Voltage fluctuations or flicker are one of the electric characteristics most complex to assess. At the time the first edition of the standard was defined [8], the vast majority of the installed WTs were fixed speed turbines (type I), which presented flicker emission values well above the expected regulatory limits [9]. However, with the use of variable speed WTs (type II) flicker emission values were reduced [10–12]. Currently, new types of WTs implement flicker mitigation strategies with the use of power electronic devices for the partial (type III) or complete (type IV) management of the generated power. This has considerably reduced the flicker emission [12–14].

36 Despite the low flicker emission of an individual WT, it is of vital importance to accurately  
37 estimate the impact of the aggregation of multiple WTs. The IEC 61000-3-7 standard defines a formula  
38 to aggregate the flicker produced by different sources. The summation exponent  $\alpha$  depends on the  
39 probability of occurrence of coincident fluctuations. The IEC 61400-21 standard specifies a quadratic  
40 summation of each individual WT value to estimate the flicker emission of a WPP. The use of a  
41 quadratic summation is based on the criteria established by the IEC 61000-3-7 standard [15], as well as  
42 on studies performed before and during the definition of the IEC 61400-21 standard [9,10,16,17].

43 Many studies have been conducted to analyze the quadratic summation of the flicker emission  
44 of WTs, based on fixed speed [9–11,16,18] or variable speed [10,11,16] WTs. Some of these studies  
45 performed measurements on two WTs assuming that the set of both turbines could be represented as  
46 the sum of the individual values [9,10,16]. Other works carried out measurements at different locations  
47 in a WPP. In [11], measurements were performed at a WT and at the end of the string feeder the WT  
48 was connected at; in [18], measurements were performed at a WT and the Point of Common Coupling  
49 (PCC) of a WPP consisting of four WTs. In both studies, flicker emission values at the string feeder or  
50 at the PCC were compared with the estimated ones obtained through the quadratic summation of the  
51 values registered at the WT. From all those studies, [10] and [11] are the only ones implementing the  
52 flicker measurement procedure of the IEC 61400-21 standard.

53 These studies reached different overall conclusions. On the one hand, [9], [10] and [16] corroborate  
54 the adequacy of the quadratic summation to estimate the flicker emission of a group of WTs. On the  
55 other hand, [18] shows important differences between the measured and estimated flicker emission  
56 values. However, these divergences could come from the fact that background fluctuations at the  
57 PCC of the WPP were not removed from the study. Finally, the results presented in [11] show that the  
58 quadratic summation provides flicker emission values higher than the measurements performed at the  
59 string feeder of the WPP.

60 In order to analyze the degree of correlation between voltage fluctuations produced by identical  
61 WTs situated in nearby locations and working under similar wind conditions, the aim of this work was  
62 twofold: to assess the flicker emission at the PCC of a WPP consisting of 16 WTs, and to analyze the  
63 quadratic summation method to estimate WPP flicker emission based on the measurements of a single  
64 WT. To that end, voltage and current waveforms were synchronously recorded at the terminals of a  
65 single WT and at the PCC of a WPP located in Spain. The estimated and measured flicker emission  
66 values were compared, and the exponent providing a better adjustment of the results was analyzed.

## 67 2. Flicker measurement procedure during continuous operation of WT

68 The IEC 61400-21 standard defines the flicker measurement and assessment procedure during  
69 continuous operation of a WT. The Maintenance Team TC88/MT21 of IEC is currently working on  
70 the modification of this procedure [19]. Figure 1 shows the block diagram of the flicker measurement  
71 procedure of the standard in force, as well as of its forthcoming edition. Both procedures comprise  
72 5 steps using the phase to neutral voltage and line current 10-min input signals recorded at the WT  
73 terminals.

74 The difference between both procedures lies in the fourth block. The standard in force specifies  
75 that each 10-min time-series has to be classified in wind speed bins according to the mean wind speed.  
76 At least fifteen 10-min time-series of voltage and current measurements have to be collected for each 1  
77 m/s wind speed bin, with bins going from a cut-in wind speed of usually 3 m/s to 15 m/s. In contrast,  
78 the forthcoming edition of the standard establishes that each 10-min time series has to be classified  
79 into power bins, according to the percentage rated power,  $P_n$ , of the WT. Moreover, eleven power bins  
80 are specified as 0, 10, 20, . . . , 100% of the  $P_n$ , being 0, 10, 20, . . . , 100 the bin midpoints. In this case, at  
81 least twenty one 10-min time-series are required for each power bin.

82 In Block 1 the interaction between the WT and an ideal grid free from voltage disturbances is  
83 implemented through the fictitious grid represented in Figure 2. The WT is modeled by means of  
84 a current generator representing the line current  $i_m(t)$  measured at the WT terminals. The grid is

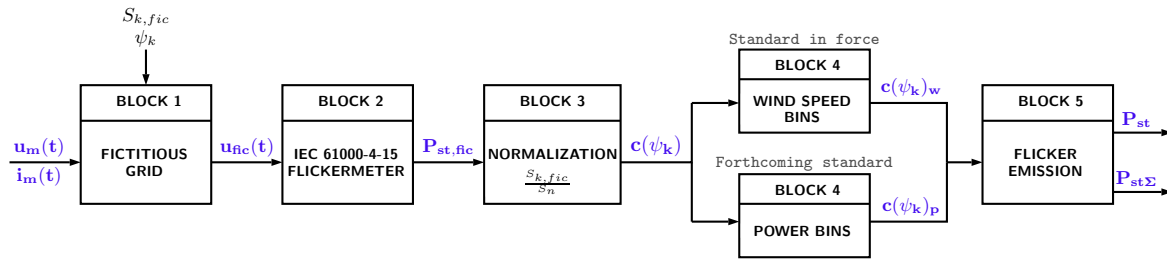


**Figure 1.** Block diagram of the measurement and assessment procedure for flicker during continuous operation of a grid connected WT according to the IEC 61400-21 standard in force and its forthcoming edition.

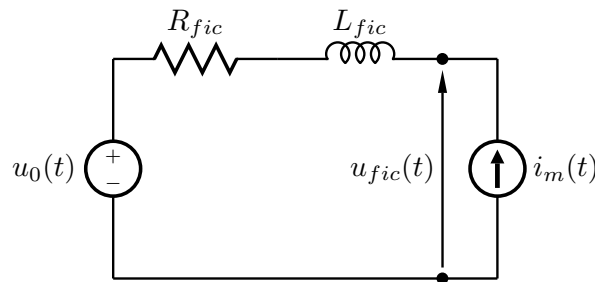


**Figure 2.** Fictitious grid implemented in Block 1 of the IEC 61400-21 standard.

85 represented by an ideal voltage generator  $u_0(t)$  connected in series with a resistance  $R_{fic}$  and an  
 86 inductance  $L_{fic}$ . The ideal voltage  $u_0(t)$  has to meet two requirements: it can not contain any voltage  
 87 fluctuations, and it shall have the same electrical angle as the voltage  $u_m(t)$  measured at the WT  
 88 terminals [20]. In this way, the fictitious voltage,  $u_{fic}(t)$ , which characterizes the voltage fluctuations  
 89 produced exclusively by the WT, is obtained according to the following equation:

$$u_{fic}(t) = u_0(t) + R_{fic} \cdot i_m(t) + L_{fic} \cdot \frac{di_m(t)}{dt}. \quad (1)$$

90 The  $u_{fic}(t)$  voltage should be obtained for four grid impedance values ( $R_{fic}$  and  $L_{fic}$ ), determined by  
 91 four grid impedance phase angles ( $\psi_k = 30^\circ, 50^\circ, 70^\circ$  y  $85^\circ$ ) and for a specific Short-Circuit Ratio (SCR).  
 92 The SCR value represents the relation between the short-circuit apparent power of the fictitious grid,  
 93  $S_{k, fic}$ , and the rated apparent power of the WT,  $S_n$ . The standard specifies a SCR value between 20 and  
 94 50. Thus, four  $u_{fic}(t)$  voltage signals are obtained for each 10-min time series input at the output of  
 95 Block 1.

96 Block 2 implements a class F1 IEC flickermeter according to the IEC 61000-4-15 standard [21],  
 97 obtaining a flicker severity value,  $P_{st, fic}$ , for each  $u_{fic}(t)$  voltage. In total, four  $P_{st, fic}$  values are obtained  
 98 for each 10-min time series, one for each  $\psi_k$  value.

99 The flicker coefficient  $c(\psi_k)$  is obtained in Block 3 by normalizing the  $P_{st, fic}$  value with the  
 100 following equation:

$$c(\psi_k) = P_{st, fic} \cdot SCR. \quad (2)$$

101 According to the standard in force, Block 4 weights the flicker coefficients  $c(\psi_k)$  of the whole set  
 102 of 10-min time-series using four annual average wind speed values. Then, the 99th percentile of each  
 103 distribution is reported, yielding 16 flicker coefficients  $c(\psi_k)_w$ . In contrast, the forthcoming edition  
 104 of the standard would require the 95th percentile of the flicker coefficients for each power bin [22],  
 105 reporting the worst case flicker coefficient  $c(\psi_k)_p$  for each  $\psi_k$  value.

106 Based on these reported values, Block 5 estimates the flicker emission from a single WT at the  
 107 PCC as follows:

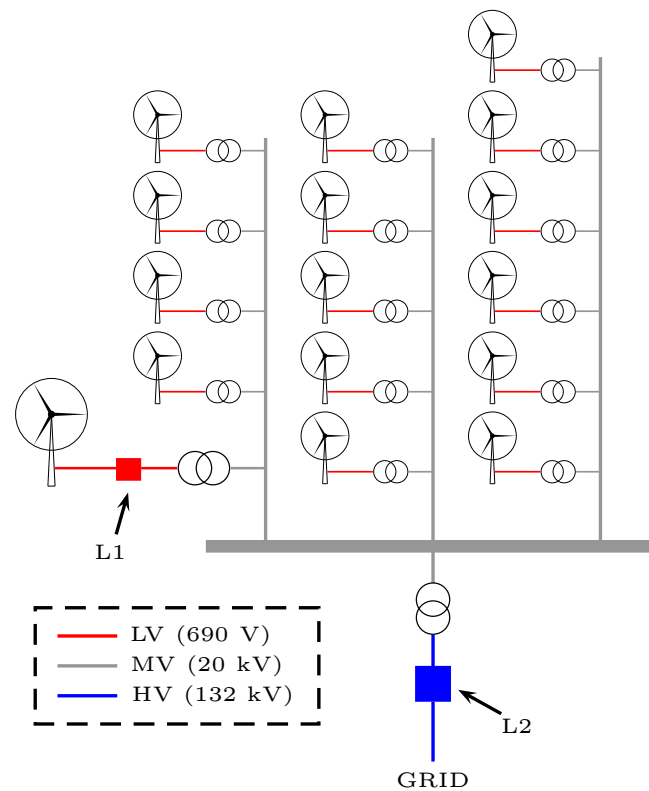


**Figure 3.** Illustration of the electrical layout of the WPP.

$$P_{st} = c(\psi_k) \cdot \frac{S_n}{S_k}, \quad (3)$$

108 where  $\psi_k$  is the grid impedance phase angle at the PCC and  $S_k$  is the short-circuit apparent power  
 109 at the PCC. In case  $\psi_k$  is not one of the values defined by the standard, a linear interpolation of the  
 110 reported values is suggested to obtain the  $c(\psi_k)$  value.

111 Finally, the standard determines that the flicker emission of a group of WTs at the PCC could be  
 112 estimated as follows:

$$P_{st,\Sigma} = \frac{1}{S_k} \cdot \sqrt{\sum_{i=1}^{N_{wt}} (c_i(\psi_k) \cdot S_{n,i})^2}, \quad (4)$$

113 where  $N_{wt}$  is the total number of WTs,  $c_i(\psi_k)$  is the individual flicker coefficient of each WT and  $S_{n,i}$   
 114 the rated apparent power of each WT.

### 115 3. Data collection

116 This work is based on a large database of real voltage and current waveforms recorded at a 32 MW  
 117 WPP located in Spain. The WPP is distributed into three strings, comprising a total of 16 Type III 2 MW  
 118 WTs disposed as shown in Figure 3.

119 Each WT is a pitch regulated, upwind WT with active yaw, three-blade rotor and a high-efficiency  
 120 4-pole doubly fed generator with wound rotor and slip rings. The WT has a rated current of 1500 A  
 121 and 690 V of nominal voltage.

122 Voltage and current GPS-synchronized measurements were performed at two different locations  
 123 of the WPP: on the low voltage side (690 V) at the terminals of one WT (L1 in Figure 3), and on the  
 124 high voltage side (132 kV) at the PCC of the WPP (L2 in Figure 3). During the month and a half long

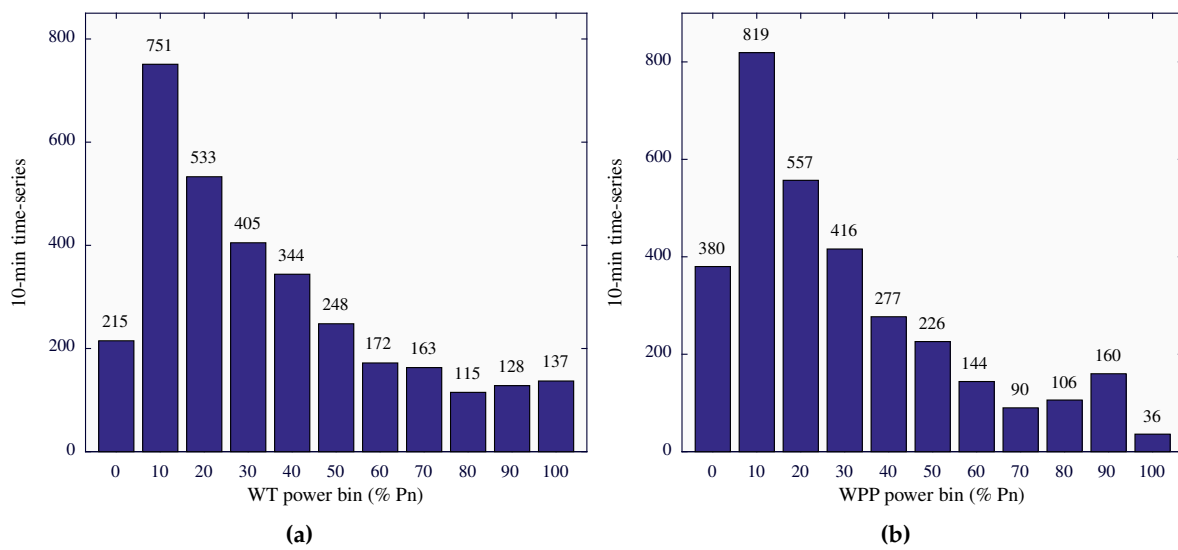


**Figure 4.** Power distribution of the selected 10-min time-series. (a) Time-series recorded at L1 with respect to the power bin of the WT (2 MW). (b) Time-series recorded at L2 with respect to the power bin of the WPP (32 MW).

125 measurement campaign, a total of 4914 10-min time-series were recorded at each location. For each  
 126 time-series the operational status of the 16 WTs was annotated and the active power at both locations  
 127 was calculated. After removing those time-series containing switching operations of the WT, and  
 128 after discarding the time-series in which not all the WTs were working, a total number of 3211 10-min  
 129 time-series were selected for the study database. Figure 4(a) shows the histogram of the time-series  
 130 power at L1, with respect to the  $P_n$  of the WT (2 MW), whereas Figure 4(b) shows the histogram of the  
 131 time-series power at L2, with respect to the  $P_n$  of the WPP (32 MW).

## 132 4. Results

133 Based on the selected 3211 time-series, flicker emission values were calculated at the PCC in two  
 134 ways: first, using the recordings from L1 and following the equation (4); second, using the recordings  
 135 from L2 and directly calculating the flicker emission. For that purpose, the impedance at the PCC was  
 136 measured, providing a value of  $Z = 6.581 \angle 87.34^\circ$ . Finally, both results were compared.

### 137 4.1. Estimation of the flicker emission at the PCC according to IEC 61400-21 standard

138 Using the voltage and current time-series recorded at L1, the  $P_{st}$  of the WT at the PCC was  
 139 calculated. To that end, equation (3) of the IEC 61400-21 procedure was applied, the measured  $S_k$   
 140 value at the PCC being 2700 MVA. Using these  $P_{st}$  values the flicker summation,  $P_{st,\Sigma}$ , was estimated  
 141 following equation (4). This equation can be simplified to  $P_{st,\Sigma} = \sqrt{16} \cdot P_{st}$ , considering that, in the  
 142 selected time-series, the 16 WTs were simultaneously working. Figure 5 represents the median, 95<sup>th</sup>  
 143 and 99<sup>th</sup> percentiles of the distribution of  $P_{st,\Sigma}$  values for each  $\psi_k$ . The maximum values were obtained  
 144 for angles between 40° and 60°. The medians of  $P_{st,\Sigma}$  distributions ranged between 0.0094 and 0.0118.  
 145 For the particular case of  $\psi_k = 87.34^\circ$ , the complete distribution is represented by means of a boxplot  
 146 in Figure 5. The edges of the blue box represent the 25<sup>th</sup> and 75<sup>th</sup> percentiles, and the black dashed  
 147 whiskers extend to the minimum and maximum values.

148 Figure 6 shows, for the case of  $\psi_k = 87.34^\circ$  and using boxplots, the distribution of  $P_{st,\Sigma}$  values for  
 149 each power bin of the WT. The central solid horizontal red line in each box is the median and the red  
 150 crosses represent the outliers of the distributions. Black circles represent the 95<sup>th</sup> percentile for each  
 151 power bin. According to the standard, these values are those to be reported as the flicker emission for  
 152 each bin.

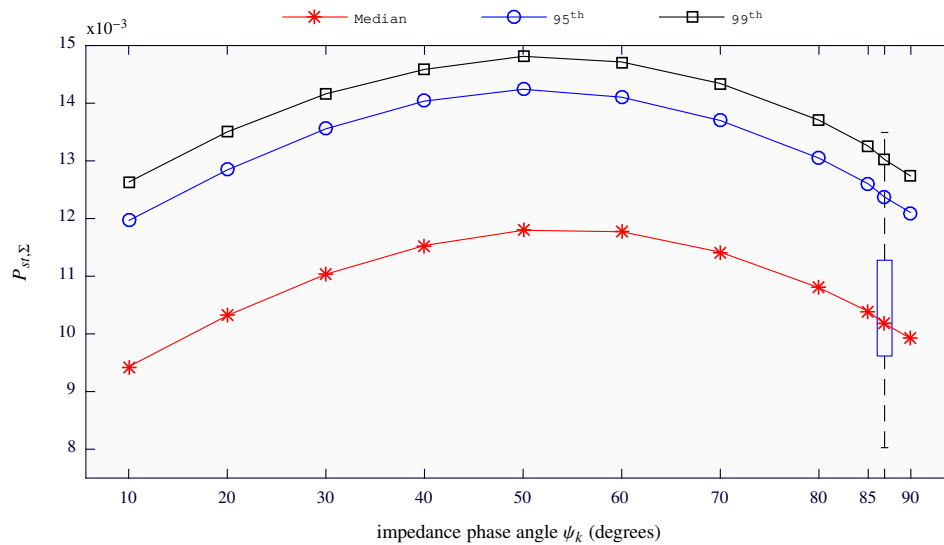


**Figure 5.** Statistics of the estimated  $P_{st,\Sigma}$  values at the PCC with respect to the  $\psi_k$  values: median (red asterisks), 95<sup>th</sup> percentile (blue circles) and 99<sup>th</sup> percentile (black squares). A boxplot is depicted to represent the distribution for the particular case of  $\psi_k = 87.34^\circ$ .

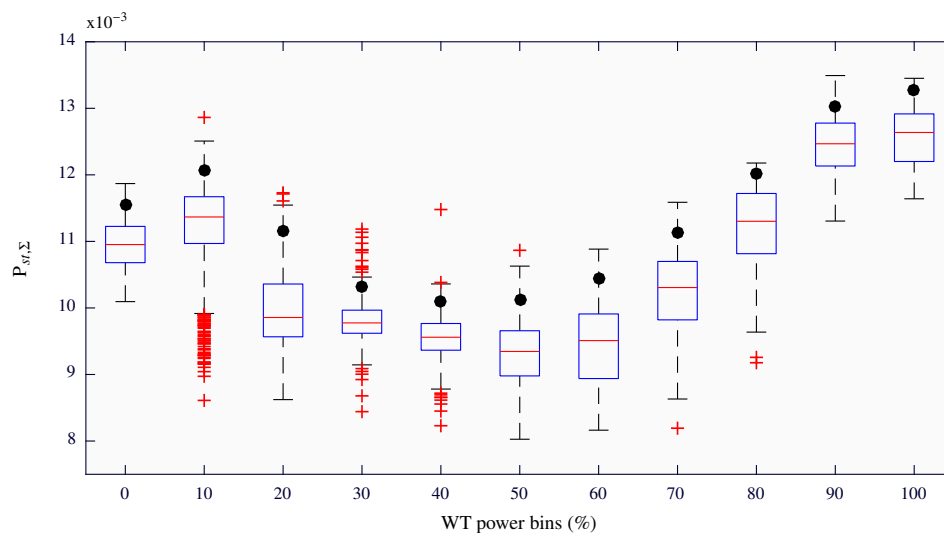


**Figure 6.** For a  $\psi_k$  value of  $87.34^\circ$ , boxplots of the estimated  $P_{st,\Sigma}$  values at the PCC with respect to the power bin of the WT (2 MW).

153 The lowest  $P_{st,\Sigma}$  values were obtained between the 30% and 60% power bins. For the lowest  
 154 power bins (0-20%) intermediate  $P_{st,\Sigma}$  values were observed. Between the 70% and 100% power bins  
 155  $P_{st,\Sigma}$  values increased as the power bin increased. Maximum values were registered between the 90%  
 156 and 100% power bins. The maximum 95<sup>th</sup> percentile was 0.0133, obtained for the 100% power bin  
 157 whose median value is 0.0126.

#### 158 4.2. Measurement of the flicker emission at the PCC

159 Using the voltage and current time-series recorded at L2, the  $P_{st,L2}$  values at the PCC of the WPP  
 160 were obtained. The direct way to obtain the flicker emission at the PCC is to analyze the registered  
 161 voltage using the IEC flickermeter. However, this procedure does not distinguish between the flicker  
 162 emission of the WPP and the background voltage fluctuations present at that measurement point in  
 163 the grid. Therefore, similarly to what the IEC 61400-21 standard establishes, the flicker emission at the  
 164 PCC exclusively produced by the WPP was obtained by means of a model representing the interaction  
 165 between the WPP and the Thevenin's equivalent circuit of the grid. In this case, the current source



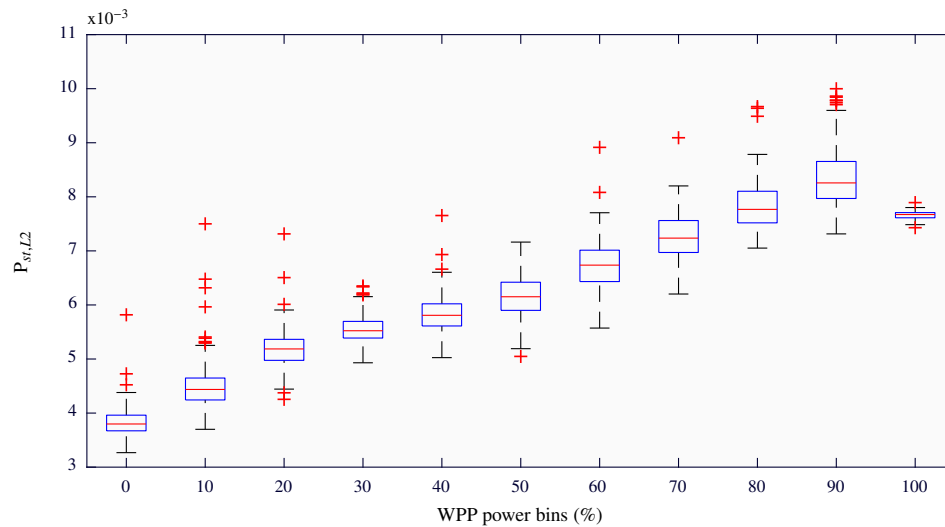


**Figure 7.** For a  $\psi_k$  value of  $87.34^\circ$ , boxplots of the measured  $P_{st,L2}$  values at the PCC (16 WTs) with respect to the power bin of the WPP (32 MW).

166 represents the current injected by the WPP whose value corresponds to the current registered at L2.  
 167 For the Thevenin impedance the known value of  $Z = 6.581|87.34^\circ$  was used.

168 Figure 7 depicts, the distributions of the measured  $P_{st,L2}$  values for each power bin of the WPP.  
 169 The obtained values ranged between 0.0033 and 0.0100, showing the low flicker emission level of the  
 170 WPP. Excluding outliers, the measured  $P_{st,L2}$  values increased as the generated power of the WPP  
 171 increased from the lowest to the 90% power bin. At this latter power bin the maximum values were  
 172 reached. The 100% power bin presented a very low dispersion and lower  $P_{st,L2}$  values compared to  
 173 the 90% power bin. It is important to note that the 100% power bin represents the situation at which  
 174 all the WTs of the WPP are working at around the 100% of their power. This implies that the flicker  
 175 generation of each WT will be practically the same and, therefore, the measured flicker values should  
 176 be similar.

#### 177 4.3. Comparison between the estimated and measured flicker emission at the PCC

178 The comparison between the estimated  $P_{st,\Sigma}$  and measured  $P_{st,L2}$  values at the PCC was performed  
 179 using the results obtained for a  $\psi_k$  angle of  $87.34^\circ$ . Overall, the measured  $P_{st,L2}$  values were lower than  
 180 the estimated ones. This proves that the standard overestimates the flicker emission of the whole WPP.

181 When comparing the corresponding individual time-series at L1 and L2, large deviations were  
 182 obtained between the measured and estimated flicker emission values. Figure 8(a) depicts the estimated  
 183 flicker values versus the measured ones. The results obtained for the time-series grouped between the  
 184 0 and 30% power bins are represented in black color, whereas the ones corresponding to power bins  
 185 between 40% and 100% are represented in red. Figure 8(b) represents, using boxplots, the distributions  
 186 of the percentage deviation between the estimated  $P_{st,\Sigma}$  and measured  $P_{st,L2}$  values, calculated as:

$$\Delta P_{st,\Sigma} = \frac{P_{st,\Sigma} - P_{st,L2}}{P_{st,L2}}. \quad (5)$$

187 From left to right, the results correspond to the time-series grouped between the 0-30%, 40-100% and  
 188 those at the 100% power bin, respectively.

189 In Figure 8(a) two different trends can be distinguished between 0-30% and 40-100% power bins.  
 190 Moreover, there is a poor correlation between the obtained results and the dashed black line which  
 191 represents the ideal situation at which the estimated and measured values are identical. However,  
 192 if only the time-series classified between 40-100% power bins are considered, a similar slope is  
 193 appreciated between the obtained results and the reference values.

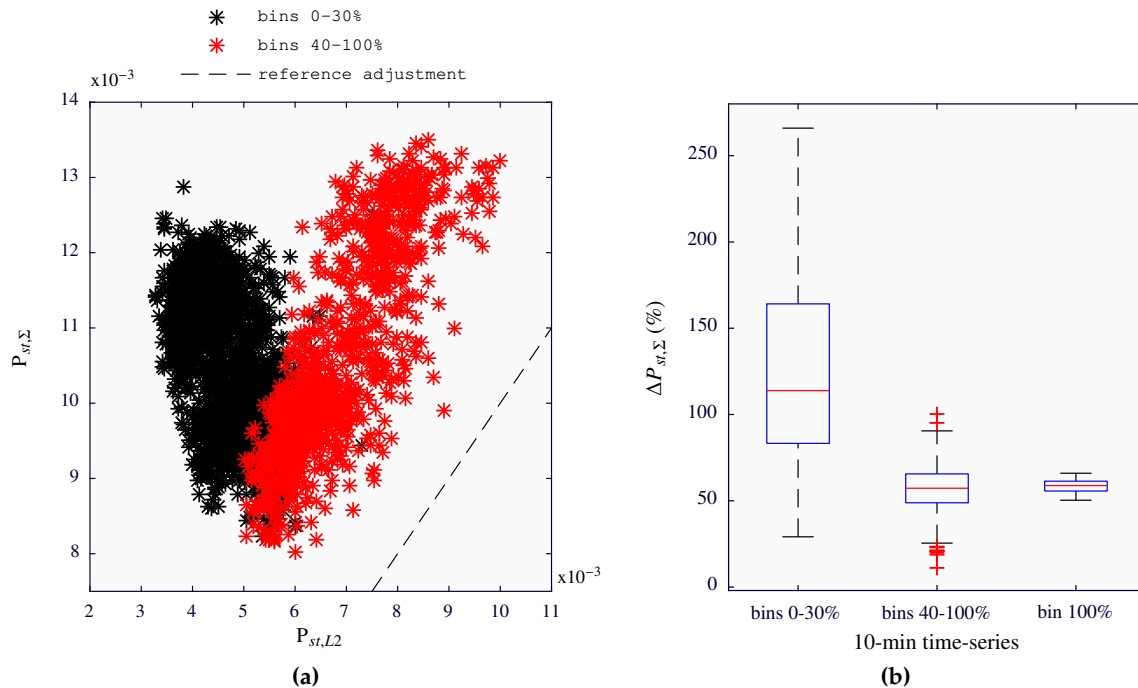


**Figure 8.** Deviation between the estimated  $P_{st,\Sigma}$  and measured  $P_{st,L2}$  values at the PCC. (a) Estimated versus measured results, obtained with the time-series classified between the power bins 0-30% (in black) and between 40-100% (in red). (b) Boxplots of the percentage deviation between the estimated  $P_{st,\Sigma}$  and the measured  $P_{st,L2}$  values.

194 Figure 8(b) shows large deviations between the estimated and measured values. For the particular  
 195 case of the results obtained for 0-30% power bins, half of the deviations were higher than 113%, with  
 196 a maximum deviation of 265%. On the other hand, for the time-series corresponding to power bins  
 197 between 40% and 100%, half of the deviations were greater than 57%, with a maximum deviation  
 198 of 100%. Considering only the time-series grouped at the 100% power bin, the deviations were  
 199 concentrated around the 59%, showing a very low dispersion.

#### 200 4.4. Summation exponent effect

201 When aggregating different flicker sources according to [15] an exponent,  $\alpha$ , is used. The value  
 202 of  $\alpha$  depends on the probability of occurrence of coincident fluctuations. Exponents  $\alpha = 1, 2,$  and  $3$   
 203 represent high, medium and low probability of occurrence, respectively, whereas  $\alpha = 4$  represents  
 204 the null probability of coincident fluctuations. Currently, the IEC 61400-21 standard in force defines  
 205 a quadratic summation to estimate the flicker caused by a whole WPP. This is because the WTs are  
 206 considered stochastic uncorrelated noise sources of flicker, and therefore present a medium probability  
 207 of occurrence of coincident fluctuations [17]. However, the effect of the exponent was studied in view  
 208 of the existing deviations.

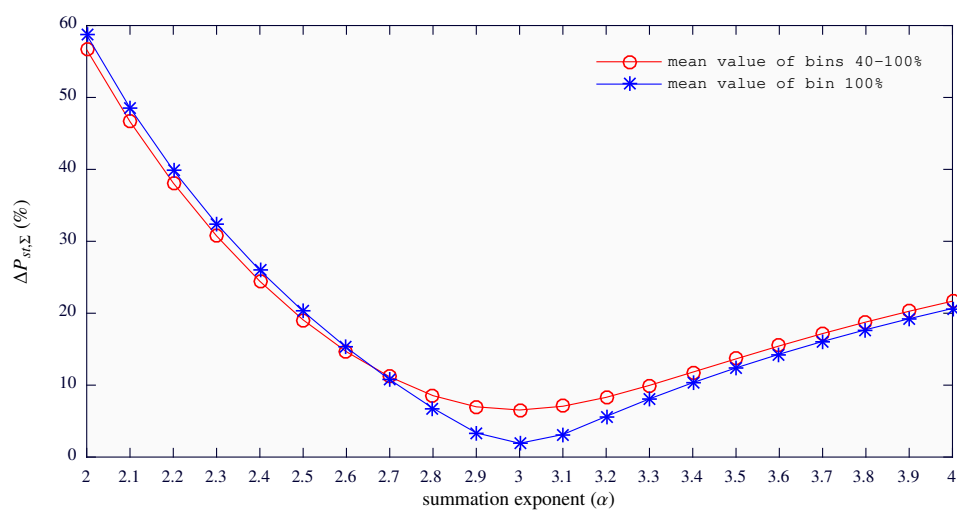
209 First, the summation exponents providing the estimated  $P_{st,\Sigma}$  values that best fit the measured  
 210  $P_{st,L2}$  values,  $\alpha_{bf}$ , have been obtained for each time-series. Table 1 shows, for each power bin, the  
 211 median and interquartile range (IQR) of the  $\alpha_{bf}$ . The IQR is represented showing the 25<sup>th</sup> and 75<sup>th</sup>  
 212 percentiles in brackets, providing a measure of the dispersion of the values. The median of the  
 213 exponents ranged between 2.75 and 8.50. For the case of power bins between 0 and 20%, the  $\alpha_{bf}$  values  
 214 presented a larger dispersion than for the rest of the bins. The 100% power bin presented the lowest  
 215 dispersion. Overall, for the time-series grouped in 40-100% power bins, the medians of  $\alpha_{bf}$  values are  
 216 around 3.

217 Second, the estimated  $P_{st,\Sigma}$  values were obtained using  $\alpha$  values between 2 and 4 in steps of 0.1.  
 218 Figure 9 shows the mean of  $\Delta P_{st,\Sigma}$  with respect to the  $\alpha$  used in the estimation. The time-series grouped



**Table 1.** Statistics of the obtained best fitting exponents,  $\alpha_{bf}$ , at each power bin of the WPP.

Bin	Best fitting exponent	
	median	IQR
0%	8.50	(7.62 - 9.91)
10%	6.23	(5.44 - 7.16)
20%	3.94	(3.70 - 4.19)
30%	3.41	(3.32 - 3.52)
40%	3.16	(3.03 - 3.28)
50%	2.97	(2.87 - 3.07)
60%	2.77	(2.66 - 2.85)
70%	2.75	(2.65 - 2.90)
80%	2.79	(2.60 - 2.85)
90%	2.86	(2.74 - 2.98)
100%	3.00	(2.94 - 3.05)

**Figure 9.** Mean of percentage deviations between the estimated  $P_{st,\Sigma}$  and measured  $P_{st,L2}$  values with respect to  $\alpha$  for the time-series grouped between the 40% and 100% power bins (red circles), and for the time-series grouped at 100% power bin (blue asterisk).

219 in the range of 40-100% power bins are represented by red circles, and the ones grouped at the 100%  
 220 power bin by blue asterisks. The lowest mean deviations were given with  $\alpha = 3$ , for both sets of  
 221 time-series.

222 Third, Figure 10 shows the obtained deviations between the estimated and measured flicker  
 223 values for the case of  $\alpha=3$ . There is a better agreement between the estimated and the measured values  
 224 for the time-series grouped between the 40% and 100% power bins. For this set of time-series the  
 225 deviations decreased to less than 10% for the 75% of the values. In the case of the 100% power bin all  
 226 deviations were below 5%.

227 Finally, the 95<sup>th</sup> percentile of the measured flicker emission value at the PCC of the WPP was  
 228  $P_{st,L2} = 0.0082$ . According to the standard, with  $\alpha=2$ , the estimated flicker emission of the WPP at the  
 229 PCC was  $P_{st,\Sigma} = 0.0133$ , based on the maximum 95<sup>th</sup> percentile of each power bin. This estimated value  
 230 presented a deviation of 62% with respect to the measured flicker emission. However, if  $\alpha=3$  is used,  
 231 an estimated flicker emission of  $P_{st,\Sigma} = 0.0084$  was obtained, with a deviation of only 2%.

## 232 5. Discussion and conclusions

233 Technological advances in the wind power sector have reduced considerably the flicker emission  
 234 of WTs [10–14]. The implementation of power control methods in modern WTs leads to the reduction  
 235 of voltage fluctuations [13,23]. These methods reduce the power fluctuations injected to the grid, and

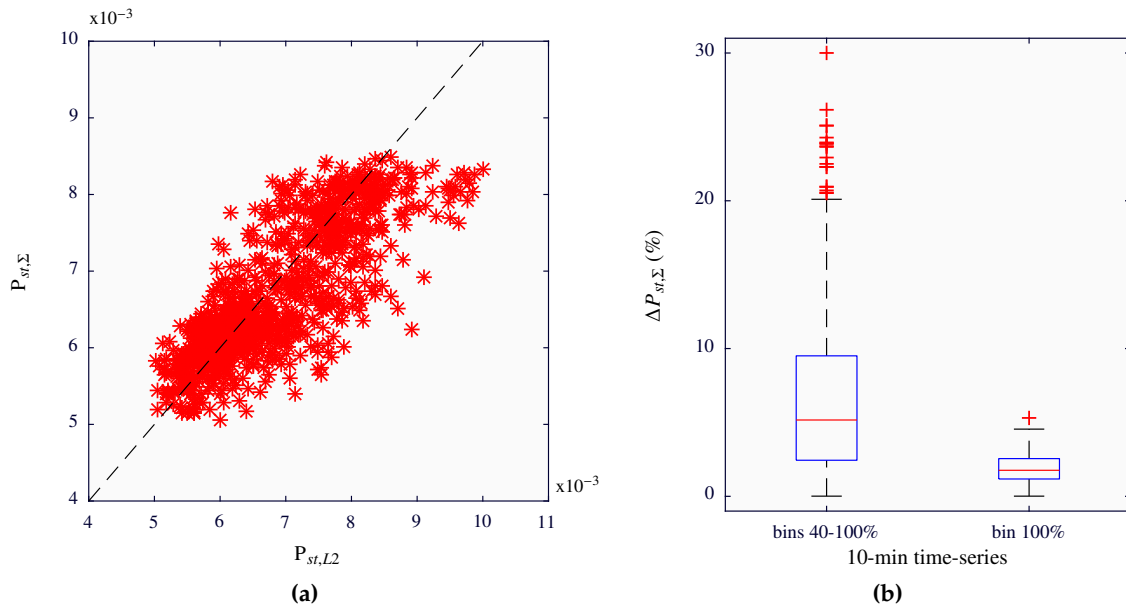


**Figure 10.** Deviation between the estimated  $P_{st,\Sigma}$  and measured  $P_{st,L2}$  values at the PCC, for  $\alpha=3$ . (a) Estimated versus measured results, obtained with the time-series classified between the power bins 40-100%. (b) Boxplots of the percentage deviation between the estimated  $P_{st,\Sigma}$  and the measured  $P_{st,L2}$  values.

236 hence also the flicker emission. As an example, the 99<sup>th</sup> percentile of the flicker coefficients  $c(85^\circ)$   
 237 reported in [12] were 5.8, 3.8 and 2.5 for WTs of types I, II and IV, respectively. The reduction in  
 238 flicker emission of these new WTs leads to think about the flicker contribution of a WPP at the PCC.  
 239 Considering the 32 MW WPP of the study, the 95<sup>th</sup> percentile of the flicker severity measured on the  
 240 voltage signal at the PCC was  $P_{st} = 0.2572$ , whereas the 95<sup>th</sup> percentile of the flicker values emitted  
 241 exclusively by the WPP at the PCC was only 0.0082. Therefore, this WPP contributes with the 3.19% of  
 242 the total flicker severity value present at the PCC. The obtained low flicker values could support that  
 243 flicker measurement is not necessary. However, the flicker emission of a WPP depends on the strength  
 244 of the grid. Thus, the same WPP will present higher or lower flicker emission values depending on the  
 245 short-circuit apparent power,  $S_k$ , at the PCC.

246 On the other hand, the IEC 61400-21 standard establishes that the estimation of the flicker emission  
 247 of a group of WTs can be estimated by means of the quadratic summation of each single flicker value  
 248 of each WT. The summation exponent  $\alpha = 2$  should be used to aggregate flicker sources that present  
 249 moderate probability of coincident fluctuations [15]. All the studies that helped to define the standard,  
 250 and those that later corroborated its validity, were based on measurements carried out at type I or  
 251 II WTs. However, the results obtained in this work suggest that the flicker aggregation in a WPP  
 252 with type III WTs should not be quadratic, but cubic. Type I and II WTs present a flicker emission  
 253 characteristic directly related to the wind speed: power fluctuations caused by variations in the wind  
 254 speed, are the ones producing flicker emission. Understandably, the effect of the wind is similar in WTs  
 255 situated in nearby locations, presenting a moderate probability of generating coincident fluctuations  
 256 between the WTs. However, type III and IV WTs implement power control systems based on power  
 257 electronics, which manage the total or partial power injection into the grid. Such power management  
 258 systems minimize the direct effect of wind fluctuations on the generated power. In fact, the flicker  
 259 emission characteristic of these types of WTs remains almost constant regardless of the wind speed.  
 260 Therefore, it seems also reasonable that with these type of WTs the probability of presenting coincident  
 261 fluctuations is lower than with type I or II WTs. According to [15], an exponent of 3 should be used  
 262 to aggregate flicker sources with low probability of coincident fluctuations. Moreover,  $\alpha = 3$  is the

263 exponent proposed by the IEC 61000-3-7 standard for general use when additional information is not  
264 available to justify a different value.

265 More studies covering different configurations of WPPs with different types of WTs are needed  
266 to confirm the results of this work. In any case, a revision of the flicker summation law currently  
267 proposed by the standard is warranted.

268 **Author Contributions:** K. Redondo have performed the experimental activity and the data processing; J.J.  
269 Gutiérrez have contributed in the conceptualization of the study; K. Redondo, J.J. Gutierrez, I. Azcarate, P. Sáiz  
270 and L.A. Leturiondo have carried out the data acquisition in the WPP; K. Redondo and I. Azcarate have prepared  
271 the first draft of the manuscript; J.J. Gutiérrez, I. Azcarate, P. Saiz and S. Ruiz de Gauna have reviewed and edited  
272 the manuscript. All the authors have approved the submitted version of this manuscript.

273 **Funding:** This research was funded by Basque Government (Basque Country, Spain) through the project IT1087-16  
274 and by the Spanish MINECO through project DPI2014-53317-R (co-financed with European FEDER funds).

275 **Conflicts of Interest:** The authors declare no conflict of interest.

## 276 Abbreviations

277 The following abbreviations are used in this manuscript:

278	GPS	Global Positioning System
	IEC	International Electrotechnical Commission
	IQR	Interquartile range
	PCC	Point of Common Coupling
279	PQ	Power Quality
	SCR	Short-Circuit Ratio
	WPP	Wind Power Plant
	WT	Wind Turbine

280

- 281 1. GWEC. Global wind report - Annual market update 2017. Technical report, Global Wind Energy Council,  
282 2018.
- 283 2. GWEC. Global wind energy outlook 2016. Technical report, Global Wind Energy Council, 2016.
- 284 3. Liang, X. Emerging Power Quality Challenges Due to Integration of Renewable Energy Sources. *IEEE*  
285 *Transactions on Industry Applications* **2017**, *53*, 855–866. doi:10.1109/TIA.2016.2626253.
- 286 4. IEC 61400-21:2008 - *Wind turbines - Part 21: Measurement and assesment of power quality characteristics of grid*  
287 *connected wind turbines*, 2 ed., 2008.
- 288 5. Abubakar, U.; Mekhilef, S.; Mokhlis, H.; Seyedmahmoudian, M.; Horan, B.; Stojcevski, A.; Bassi,  
289 H.; Hosin Rawa, M.J. Transient Faults in Wind Energy Conversion Systems: Analysis, Modelling  
290 Methodologies and Remedies. *Energies* **2018**, *11*, 2249. doi:10.3390/en11092249.
- 291 6. García, H.; Segundo, J.; Rodríguez-Hernández, O.; Campos-Amezcuca, R.; Jaramillo, O. Harmonic  
292 Modelling of the Wind Turbine Induction Generator for Dynamic Analysis of Power Quality. *Energies* **2018**,  
293 *11*, 104. doi:10.3390/en11010104.
- 294 7. Sellami, T.; Berriri, H.; Jelassi, S.; Darcherif, A.M.; Mimouni, M.F. Short-Circuit Fault Tolerant Control of  
295 a Wind Turbine Driven Induction Generator Based on Sliding Mode Observers. *Energies* **2017**, *10*, 1611.  
296 doi:10.3390/en10101611.
- 297 8. IEC 61400-21:2001 - *Wind Turbine Generator Systems - Part21: Measurement and Assessment of Power Quality*  
298 *Characteristics of Grid Connected Wind Turbines*, 1 ed., 2001.
- 299 9. Sorensen, P.; Tande, J.O.; Sondergaard, L.; Kledal, J.D. Flicker Emission Levels from Wind Turbines. *Wind*  
300 *Engineering* **1996**, *20*, 39–46.
- 301 10. Larsson, A. Flicker emission of wind turbines during continuous operation. *Energy Conversion, IEEE*  
302 *Transactions on* **2002**, *17*, 114–118.
- 303 11. Barahona, B.; Sorensen, P.; Christensen, L.; Sorensen, T.; Nielsen, H.; Larsen, X. Validation of the Standard  
304 Method for Assessing Flicker From Wind Turbines. *Energy Conversion, IEEE Transactions on* **2011**, *26*, 373  
305 –378. doi:10.1109/TEC.2010.2068299.

- 306 12. Christensen, L.; Sorensen, P.; Sorensen, T., T.; Nielsen, H. Evaluation of Measuring Methods for Flicker  
307 Emission from Modern Wind Turbine; AEE: Madrid, Spain, 2009.
- 308 13. Ammar, M.; Joos, G. Impact of Distributed Wind Generators Reactive Power Behavior on Flicker Severity.  
309 *IEEE Transactions on Energy Conversion* **2013**, *28*, 425–433. doi:10.1109/TEC.2013.2256425.
- 310 14. Chen, Z.; Guerrero, J.; Blaabjerg, F. A Review of the State of the Art of Power Electronics for Wind Turbines.  
311 *IEEE Transactions on Power Electronics* **2009**, *24*, 1859–1875. doi:10.1109/TPEL.2009.2017082.
- 312 15. IEC 61000-3-7:2008 - *Electromagnetic compatibility (EMC) - Part 3-7: Limits - Assessment of emission limits for*  
313 *the connection of fluctuating installations to MV, HV and EHV power systems*, 2 ed., 2008.
- 314 16. Sorensen, P.; Pedersen, T.F.; Gerdes, G.; Klosse, R.; Santjer, F.; Robertson, N.; Davy, W.; Koulouvari, M.;  
315 Morfiadakis, E.; Larsson, A. European Wind Turbine Testing Procedure Developments Task 2: Power  
316 Quality. Technical Report, Riso National Laboratory, Denmark, 2001.
- 317 17. Sorensen, P. Methods for calculation of the flicker contributions from wind turbines. Technical Report  
318 Riso-I-939(EN), Riso National Laboratory, Roskilde, Denmark, 1995.
- 319 18. Thiringer, T.; Petru, T.; Lundberg, S. Flicker Contribution From Wind Turbine Installations. *IEEE*  
320 *Transactions on Energy Conversion* **2004**, *19*, 157–163. doi:10.1109/TEC.2003.816604.
- 321 19. Andresen, B.; Sørensen, P.; Santjer, F.; Niiranen, J. Overview, status and outline of the new revision for  
322 the IEC 61400-21 – Measurement and assessment of power quality characteristics of grid connected wind  
323 turbines. 12th Int. Workshop on Large-Scale Integr. of Wind Power into Power Syst., 2013.
- 324 20. Redondo, K.; Lazkano, A.; Saiz, P.; Gutierrez, J.J.; Azcarate, I.; Leturiondo, L.A. A strategy for improving  
325 the accuracy of flicker emission measurement from wind turbines. *Electric Power Systems Research* **2016**,  
326 *133*, 12–19. doi:10.1016/j.epsr.2015.11.040.
- 327 21. IEC 61000-4-15 - International Electrotechnical Commission. *Electromagnetic Compatibility (EMC) - Part 4:*  
328 *Testing and Measurements Techniques - Section 15: Flickermeter Functional and Desing Specifications*, 2 ed., 2010.
- 329 22. Lazkano, A.; Redondo, K.; Gutierrez, J.; Saiz, P.; Leturiondo, L.; Azkarate, I. Revision of the  
330 standard method for statistical evaluation of flicker coefficients in wind turbines. 2014 IEEE  
331 16th International Conference on Harmonics and Quality of Power (ICHQP), 2014, pp. 258–262.  
332 doi:10.1109/ICHQP.2014.6842745.
- 333 23. She, X.; Huang, A.; Wang, F.; Burgos, R. Wind Energy System With Integrated Functions of Active Power  
334 Transfer, Reactive Power Compensation, and Voltage Conversion. *IEEE Transactions on Industrial Electronics*  
335 **2013**, *60*, 4512–4524. doi:10.1109/TIE.2012.2216245.